Draft version August 10, 2025
Typeset using LaTeX **modern** style in AASTeX631

Hiding Out at the Low End: No Gap and a Peak in the Black-Hole Mass Spectrum

Anarya Ray,[1,2] Will M. Farr,[3,4] and Vassiliki Kalogera[1,2,5]

[1] *Center for Interdisciplinary Exploration and Research in Astrophysics (CIERA), Northwestern University, 1800 Sherman Ave, Evanston, IL 60201, USA*

[2] *The NSF-Simons AI Institute for the Sky (NSF-Simons SkAI), 875 N. Michigan Ave., Suite 4010, Chicago, IL 60611*

[3] *Department of Physics and Astronomy, Stony Brook University, Stony Brook, NY 11794, USA*

[4] *Center for Computational Astrophysics, Flatiron Institute, 162 Fifth Avenue, New York, NY 10010, USA*

[5] *Department of Physics and Astronomy, Northwestern University, 2145 Sheridan RD, Evanston, IL 60208, USA*

ABSTRACT

In recent years, the existence of a gap in the mass spectrum of compact objects formed from stellar collapse, between the heaviest neutron stars and the lightest black holes, has been a matter of significant debate. The presence or absence of a mass gap has implications for the supernova mechanism, as well as being a fundamental property of the compact object mass function. In X-ray binaries containing black holes a gap is observed, but it is not known whether this is representative of a true gap in the mass function or due to selection effects or systematic biases in mass estimation. Binary black hole mergers detected from gravitational waves in the GWTC-3 transient catalog furnish a large sample of several tens of low-mass black holes with a well-understood selection function. Here we analyze the 25 GWTC-3 merger events (along with GW230529_181500) with at least one black hole ($3\,M_\odot < m_1$) and chirp masses below those of a $20\,M_\odot$–$20\,M_\odot$ merger ($\mathcal{M} < 17.41\,M_\odot$) to uncover the structure of the low-mass black hole mass function. Using flexible parameterized models for the mass function, we find, similar to existing studies, a sharp peak in the mass function at $m \simeq (8 - 10 M_\odot)$. We observe a steady decline in the merger rate to lower masses, but by less than an order of magnitude in total, and find that the first percentile of black hole masses in our most flexible model is $m_{1\%} = 3.13^{+0.23}_{-0.05}\,M_\odot$. In other words, this sample of low-mass black holes is not consistent with the existence of a mass gap.

anarya.ray@northwestern.edu
will.farr@stonybrook.edu
wfarr@flatironinstitute.org
vicky@northwestern.edu

1. INTRODUCTION

The existence of a gap in the compact object mass-spectrum between the lightest black holes and the heaviest neutron stars remains an open question with far-reaching implications. Observational evidence for the presence or absence of a *lower-mass gap* in the population of compact objects formed from stellar collapse can offer new insights into the universal properties of dense matter and the uncertain mechanisms of supernova explosions (Fryer & Kalogera 2001; Fryer et al. 2012; Mandel & Müller 2020; Zevin et al. 2020; Liu et al. 2021; Patton et al. 2022; Siegel et al. 2023). In addition, as a fundamental property of the compact object mass spectrum, the lower-mass gap will likely play a vital role in cosmological explorations using gravitational wave (GW) observations from future detectors (Ezquiaga & Holz 2022).

Several studies relying on electromagnetic observations of low-mass X-ray binaries (LMXBs) have reported the existence of the lower mass gap (Bailyn et al. 1998; Ozel et al. 2010; Farr et al. 2011). They have shown that Bayesian inference of phenomenological population models for compact object masses yields a posterior distribution for minimum black-hole mass, which can be constrained given data. Using growing samples of LMXB observations and a variety of mass-distribution models, they have found with 90% posterior probability that the minimum BH mass is $\simeq 4.5 M_\odot$ or higher, which suggests the existence of a gap between the heaviest possible non-rotating NSs ($2-3M_\odot$, Rhoades & Ruffini 1974; Kalogera & Baym 1996; Mueller & Serot 1996; Özel & Freire 2016; Margalit & Metzger 2017; Ai et al. 2019; Shao et al. 2020; Raaijmakers et al. 2021) and the lightest observed BHs. If true, these findings are indicative of the observational preference of rapid supernova instability time scales ($\sim 10ms$, Fryer et al. 2012; Belczynski et al. 2012; Fryer et al. 2022; Siegel et al. 2023)

However, the analyses above are susceptible to several systematic biases, which we summarize as follows. Firstly, various assumptions underlying emission models of accretion flows can significantly bias the measured BH masses, which can in turn affect the conclusions about a gap (Kreidberg et al. 2012). On the other hand, substantial selection biases can be incurred through the incorrect assumption that every draw from their mass distribution model is equally likely to be observable (Farr et al. 2011; Siegel et al. 2023). Relying on a forward modeling approach towards LMXB formation, a recent study by Siegel et al. (2023) has shown that for supernova mechanisms capable of producing BHs in the gap, transient LMXB selection effects can significantly bias the observable sample (see also, for example, Liotine et al. 2023, for similar effects of selection biases in high mass X-ray binary populations). Hence, it is unclear whether or not existing LMXB-based measurements of the minimum BH mass can be considered unbiased observational evidence of an existent lower mass gap. The difficulty in modeling transient LMXB selection effects, and the possibility of systematic errors in single source mass measurements, therefore necessitates alter-

native probes of the compact object mass spectrum to ascertain the existence of a lower mass gap.

Observations of GWs from compact binary coalescences (CBCs) by the LIGO-Virgo-KAGRA (LVK, Aasi et al. 2015; Acernese et al. 2015; Akutsu et al. 2021) detector network offer a novel way to probe the existence of a lower mass gap that is free of such systematic biases (Farah et al. 2022; Abac et al. 2024; Abbott et al. 2023a). Selection effects in GW observations are well understood and easily modeled through the recovery of simulated sources injected into detector noise realizations (Thrane & Talbot 2019; Mandel et al. 2019; Wysocki et al. 2019), which can then be used to obtain the astrophysical mass distribution of compact objects as compared to the observed distributions inferred by LMXB investigations. Previous studies have attempted this exploration by analyzing all CBC observations (including NS containing events) using a mass distribution model that allows for a shallow gap (Farah et al. 2022; Abbott et al. 2023a; Abac et al. 2024). The location, depth, and width of the gap were inferred a posteriori, and Bayesian evidences were computed for values of these parameters that correspond to the presence and absence of a lower gap.

Farah et al. (2022) have found from the second gravitational wave transient catalog (Abbott et al. 2021) that the parameters controlling the gap-like feature built into their mass distribution model have a posteriori values that prefer the existence of a lower mass gap with a Bayes factor of 55.0 over its absence. Subsequent studies by Abbott et al. (2023a) and Abac et al. (2024) have updated this number to lower values by including events from the third gravitational wave transient catalog (GWTC-3, Abbott et al. 2023b) and the mass-gap event GW230529_181500 (a compact binary merger whose most massive component lies in the $3 - 5M_{\odot}$ mass range, Abac et al. 2024). Abbott et al. (2023a) have further reported that there is no significant observational preference in GWTC-3 for or against models that exhibit or rule out a lower mass gap as compared to a default mass distribution model, which is agnostic of any gap-like feature in the relevant mass range.

It is to be noted, however, that in addition to the difference in the treatment of selection biases, existing GW-based studies have explored a fundamentally different property of the compact object mass spectrum than the LMXB investigations, on which we elaborate as follows. The LMXB dataset comprises of observed systems whose only compact object components are BHs (more massive than the heaviest possible non-rotating NS), with the corresponding analyses attempting to constrain the minimum mass of BHs either as a cutoff or percentile of the inferred BH mass function (Bailyn et al. 1998; Ozel et al. 2010; Farr et al. 2011). The GW analyses have instead tried to model and identify a dearth of binary mergers in the full compact object mass spectrum, near the maximum NS mass, using a dataset of observed systems that comprise both BHs and/or NSs (i.e. including BNS systems, Farah et al. 2022; Abbott et al. 2023a; Abac et al. 2024). *Hence, direct comparison of existing GW and LMXB-based probes of the lower mass gap might not be fully justified given the*

fundamental difference between these approaches in their definitions of the lower-mass gap as a property of the compact object mass spectrum.

In this paper, using flexibly parametrized population models, we analyze GW observations of CBCs whose BH components are more massive than the heaviest possible NSs and constrain the minimum BH mass as a percentile of the inferred BH mass function (similar to the approach of X-ray binary studies, Farr et al. 2011)[1]. By relying on a mass cut (Roy et al. 2025) to prevent NS components from contaminating our analysis and using a generic model for the BH mass spectrum, we constrain the first percentile of the BH mass function to be $\sim 3M_\odot$ at 90% confidence, given data from GWCT3 and GW230529_181500. Our models respond to the overall abundance of mergers with black holes in the mass range just above that of the heaviest neutron stars, and not to any explicitly modeled gap-like feature in the distribution functions. We show that our results are robust against reasonable variations of the mass-cut imposed during event selection and of the functional forms of the population models used in the analysis. The discrepancy between our measurements of the minimum BH mass and that of LMXB studies can therefore be attributed either to the differences in the treatment of selection effects, systematic biases in LMXB mass measurements, or potentially to that in the evolutionary pathways of LMXBs and BH containing CBC systems, or to systematic mis-estimation of masses in at least some LMXB systems.

This paper is organized as follows. In Sec. 2, we describe our population model, analysis framework, and event selection method. In Sec. 3 we show our main results and discuss potential sources of systematics. In Sec. 4 we discuss the implications of our study and then conclude in Sec. 4 with as summary of the main results and the scope of potential follow-up investigations.

2. METHODS

We construct flexible population models for low-mass BBHs and analyze a sample of 25 GWTC-3 observations, both with and without GW230529_181500, to investigate features in the mass-function and assess whether or not a gap is necessary to fit the observed dataset. The population inference and event selection methods used to carry out this exploration are delineated as follows.

2.1. *Population Model*

We model the BH mass function as a part of the compact object mass spectrum above the maximum possible NS mass ($m_{\rm low}$) which we fix throughout the analysis. To explore the low-mass BH population, we define our mass functions as follows:

$$m_1 m_2 \frac{\mathrm{d}N}{\mathrm{d}m_1 \mathrm{d}m_2 \mathrm{d}V \mathrm{d}t} = R(z) f\left(m_1\right) f\left(m_2\right) g(m_1, m_2). \tag{1}$$

The function f represents the "common" mass function for both components in a binary, and includes a contribution to account for neutron stars, $f_{\rm NS}$, with masses

[1] See Sec. 2 for a discussion regarding the robustness of percentile measurements given the size of the dataset.

below $m_{\rm low}$; and a contribution for black holes with masses above $m_{\rm low}$, $f_{\rm BH}$:

$$f(m) = \begin{cases} f_{\rm NS}(m) & m < m_{\rm low} \\ f_{\rm BH}(m) & m_{\rm low} < m. \end{cases} \tag{2}$$

The neutron star component is modeled with a Gaussian shape (a reasonable approximation to the mass function of binary neutron stars observed in our Galaxy (Farr & Chatziioannou 2020; Alsing et al. 2018)), with a peak at $\mu_{\rm NS}$, a width $\sigma_{\rm NS}$, and a rate density at $m = \mu_{\rm NS}$ (relative to the black hole component; see below) of $r_{\rm NS}$:

$$f_{\rm NS}(m) = r_{\rm NS} \exp\left(-\frac{(m-\mu_{\rm NS})^2}{2\sigma_{\rm NS}^2}\right). \tag{3}$$

The black hole component is either a broken power law with break mass m_b and power law indices α_1 and α_2 below and above the break:

$$f_{\rm BH}(m) = \begin{cases} \left(\frac{m}{m_b}\right)^{\alpha_1} & m < m_b \\ \left(\frac{m}{m_b}\right)^{\alpha_2} & m_b < m \end{cases}, \tag{4}$$

or a sum of a broken power law and a Gaussian shape peaking at the break mass (each contributing a fraction $1 - f_g$ and f_g to the rate density at the break / peak mass):

$$f_{\rm BH}(m) = f_g \exp\left(-\frac{(m-\mu)^2}{2\sigma^2}\right) + (1-f_g) \begin{cases} \left(\frac{m}{\mu}\right)^{\alpha_1} & m < \mu \\ \left(\frac{m}{\mu}\right)^{\alpha_2} & \mu < m \end{cases}. \tag{5}$$

In both cases, $f_{\rm BH}(m) = 1$ when $m = m_b$ or $m = \mu$, supporting that $r_{\rm NS}$ is the merger rate denisty at the peak of the neutron star component *relative* to the peak of the black hole component.

The "pairing function" (Fishbach & Holz 2020) g is a power law in the total mass,

$$g(m_1, m_2) = \left(\frac{1 + \frac{m_2}{m_1}}{2}\right)^{\beta}. \tag{6}$$

Note that this choice of pairing function, in contrast to a power-law pairing (Abbott et al. 2023a), implies that for $\beta \neq 0$ the mass function is not *separable* into a function of m_1 and a function of m_2. We also explored Gaussian pairing functions,

$$g\left(m_1, m_2\right) \propto \exp\left(-\left(m_2/m_1 - \mu_q\right)^2 / \left(2\sigma_q^2\right)\right); \tag{7}$$

but found no qualitative and few quantitative differences with the results reported here.

The merger rate evolves in redshift according to $R(z)$ with

$$R(z) = R_0 \left(1 + \left(\frac{1}{1+z_p}\right)^{\kappa}\right) \frac{(1+z)^{\lambda}}{1 + \left(\frac{1+z}{1+z_p}\right)^{\kappa}}, \tag{8}$$

with fixed $z_p = 1.9$, $\kappa = 5.6$, and $\lambda = 2.7$, following Madau & Dickinson (2014). For a low-mass sample like we analyze here, it is appropriate to fix the redshift evolution of the merger rate, since such mergers are only observable to low redshift, giving a small "lever arm" to constrain the redshift evolution.

With these definitions, R_0 is the merger rate per natural log mass squared, per comoving volume, per time at redshift $z = 0$, $m_1 = m_2 = \mu, m_b$. We use the convention $m_2 \leq m_1$. The parameter α_1 is the power law index of the common mass function below (power law) or well below (i.e. several σ; power law plus Gaussian) the peak of the BH mass function, and α_2 the power law slope above. Our population distribution is completely determined by 8 *hyperparameters* for the broken-power-law (BPL) model $\vec{\lambda} = (\mu_{NS}, \sigma_{NS}, r_{NS}, \alpha_1, \alpha_2, m_b, \beta, R_0)$, with the broken-power-law+Gaussian (BPLG) model requiring three additional quantities f_g, μ, σ.

Given measurements of these hyper-parameters, the "common" mass function f can be normalized to obtain a probability distribution for $m_{\rm low} \leq m \leq m_{\rm high}$ which can be written as:

$$p(m) \equiv \frac{f(m)}{\int_{m_{\rm low}}^{m_{\rm high}} {\rm d}m'\, f(m')}. \tag{9}$$

Denoting $m_{1\%}$ to be the first percentile of this distribution, we can rely on its measurements to infer the minimum BH mass and hence the existence of a lower mass-gap (Farr et al. 2011).

We note that given the sample-size ($O(20-30)$) of events analyzed with this framework, reasonable measurement of the first percentile are obtainable. For such sample-sizes, according to the finite-sample extension of Chebychev's inequality (Saw et al. 1984; Kabán 2012), the first percentile of a distribution will be less than roughly 10 times the sample-standard-deviation away from the sample-mean. Hence, the reliability of percentile measurements from such a finite set of samples depends on that of the mean and standard deviation, which can both be reliably constrained from O(20-30) observations, within model assumptions. We show that the conclusions obtained from our $m_{1\%}$ measurements are consistent between reasonable variations of both the functional forms of our distribution functions as well as the chosen values of m_{low}.

2.2. *Bayesian Hierarchical Inference*

To infer the hyperparameters characterizing our mass function models, we employ Bayesian hierarchical methods on our selection of GWTC-3 events (described below). Merging BBHs constitute an inhomogeneous Poisson process. Modeling such a process subject to observations with measurement uncertainty and selection effects is described Mandel et al. (2019); Vitale et al. (2020); Loredo (2004); Wysocki et al. (2019). Note that here we do not model the distribution of CBC spin parameters which amounts to fixing the same to the uninformative priors used during single event PE, which are isotropically oriented component spins distributed uniformly in magnitude (Abbott et al. 2023a).

We impose uniform priors on all hyperparameters. We use Hamiltonian Monte-Carlo methods, specifically the No U Turn Sampler (NUTS, Neal 2011; Homan & Gelman 2014), to sample from the population model posterior. To ensure quick and efficient computation of the selection function normalization (Mandel et al. 2019), we reweight the detectable sample of simulated events provided by the LVK (Abbott et al. 2023a) to a base line population model that corresponds to a fiducial value of the hyperparameters. We monitor convergence of the Monte-Carlo sums used to compute the selection normalization and average over single-event likelihoods (Farr 2019; Essick & Farr 2022; Talbot & Golomb 2023)

2.3. *Mass cuts and Event Selection*

With the primary goal of constraining the minimum BH mass, we chose our dataset of low mass BH that are confidently detectied (false alarm rate from at least one LVK pipeline lower than $1\,\mathrm{yr}^{-1}$ Abbott et al. (2023a)) containing GW events based on the following mass-cuts:

$$m_{\rm low} \leq m_1 \;\&\; \mathcal{M} \leq \mathcal{M}_{\rm max}. \tag{10}$$

While the lower cut on primary mass is necessary to ensure that we are modeling features of the BH mass function, the upper cuts on chirp mass are imposed to remove events that are not expected to contribute to the inference of the low-mass BBH population. Our canonical analysis uses $(3M_\odot, 17.41\,M_\odot)$ respectively for $(m_{\rm low}, M_{c,\rm max})$. Out of these bounds we expect $m_{\rm low}$ to have the most significant impact on the inference of $m_{1\%}$. We study the systematic changes in $m_{1\%}$ due to variations in $m_{\rm low}$ by re-running the analysis with different choices of $m_{\rm low}$ values near $3M_\odot$ and comparing the corresponding $m_{1\%}$ posteriors.

To restrict to low-mass events, we impose the requirement that 50% of posterior samples for each event lie within our chosen mass-cuts (Roy et al. 2025). Technically speaking, because the posterior distribution sampled by parameter estimation is a function of the data, these cuts satisfy the model assumptions of the selected population models in Mandel et al. (2019); but to properly implement the normalization necessary to correct for selection, we would need to perform similar parameter estimation on the LVK sample of detected injections (Abbott et al. 2023a; Roy et al. 2025), which is extremely challenging. Instead, we choose to implement our cuts in chirp mass, a fairly well-measured variable, and treat the detected injections asymmetrically to the catalog events, rejecting any injection whose true parameter values lie outside our mass cut. See Fig, 1 for a visualization of our mass cuts in the $m_1 - m_2$ parameter space and the posterior distributions of the selected events; because chirp mass is so well-measured, only one event's inclusion in the analysis set depends in any meaningful way on the 50% threshold chosen (i.e. for all but one event, our mass cuts are equivalent to imposing the same cut on the—unknown—true masses). During inference, we further impose $(dN/dm_1dm_2dz) = 0$ outside of the cuts and normalize the distributions accordingly.

In other words, we are inferring our mass function from a dataset of CBCs that contain at least one BH (a compact object heavier than $m_{\rm low}$) and constraining the minimum BH mass as a percentile of this distribution after normalizing it in between $m_{\rm low} < m < m_{\rm high}$ (see Eq. (9)). This justifies a direct comparison of our measurements with LMXB studies (Bailyn et al. 1998; Farr et al. 2011; Ozel et al. 2010) which also attempt to constrain the minimum BH mass from a dataset of observed systems whose only compact object components are BHs, in contrast to other GW-based studies (Farah et al. 2022) which instead look for a dearth in the full compact object mass spectrum near the maximum NS mass from a dataset of BNS, NSBH, and BBH systems.

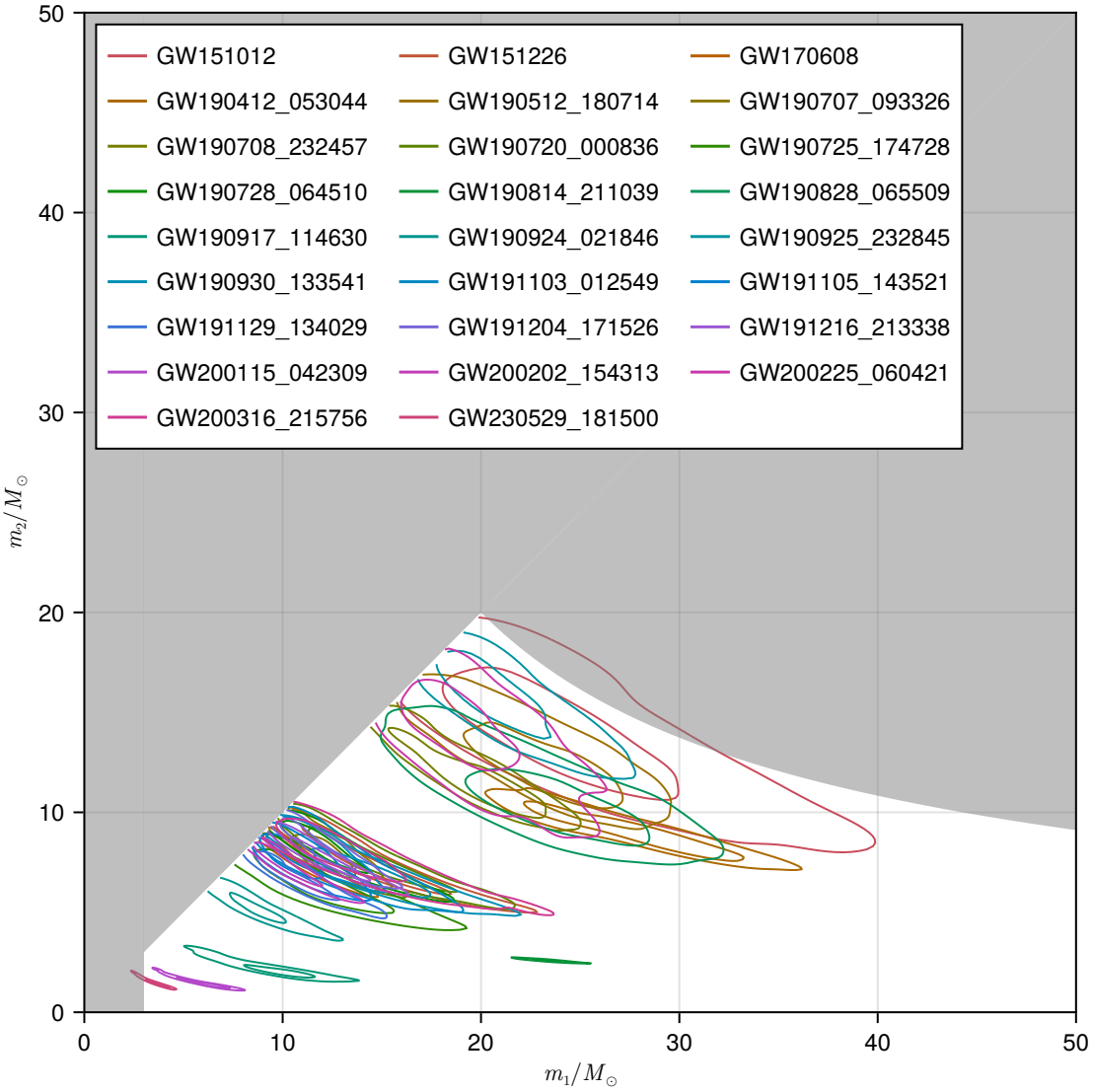

Figure 1. Contour plot of the likelihood functions for the primary and secondary black hole masses in the events considered in this analysis. The contours show credible regions containing 50% and 90% of the likelihood for each event. The dashed lines show our selection cuts, with $m_1 > 3\,M_\odot$ and $\mathcal{M} < 17.41\,M_\odot$.

3. RESULTS

In this section, we present our results obtained from the 25 GWTC-3 events that satisfy our detection threshold (i.e. a false alarm rate of less than one per year) and mass-cuts along with the mass gap event GW230529_181500. We use single-event posterior samples publicly released by the LVK (Abbott et al. 2023c; LIGO Scientific Collaboration et al. 2024) for each observation to construct our likelihood. We also use LVK's publicly released set of detectable injections (Abbott et al. 2023c) to correct for selection biases in the analysis (Mandel et al. 2019). Note that this set of detectable simulations estimates detector sensitivity through the LVK's third

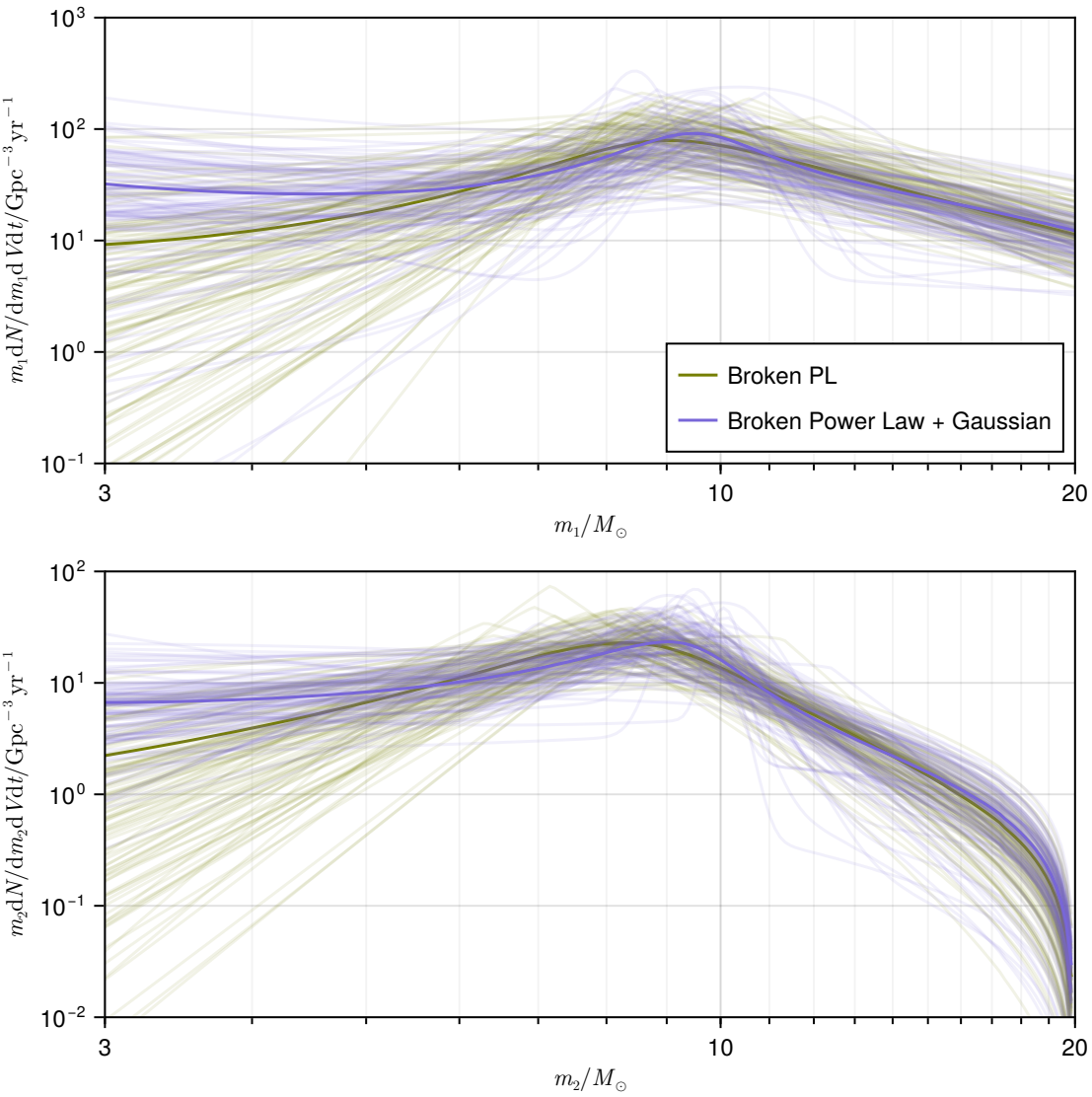

Figure 2. Inferred mass functions for $3\,M_\odot < m_2 < m_1 < 20\,M_\odot$ from two models; both primary and secondary (marginal) mass functions are shown. Dark lines show the posterior mean mass function; light lines are individual draws from the posterior over mass functions.

observation run which we expect to suffice since GW230529_181500 was detected within the first two weeks of the fourth observing run (Abac et al. 2024).

In Fig. 2, we show the inferred distributions of individual component BH masses and In Fig. 3, the common BH mass function of Eq. (9). Using both of our models we find a strong excess of BHs near $m = 9.31^{+0.73}_{-0.93}\,M_\odot$, with an overall merger rate density of $96^{+119}_{-52}\,\mathrm{Gpc}^{-3}\,\mathrm{yr}^{-1}$per log mass squared, with the numbers corresponding to the BPLG model. The merger rate density is found to fall off by nearly an order of magnitude on either side of this peak. We find that our models tend to disagree towards the lower end of the mass spectrum with the BPL model predicting a sharper drop in merger rate density. This behavior is expected given the lower flexibility of the

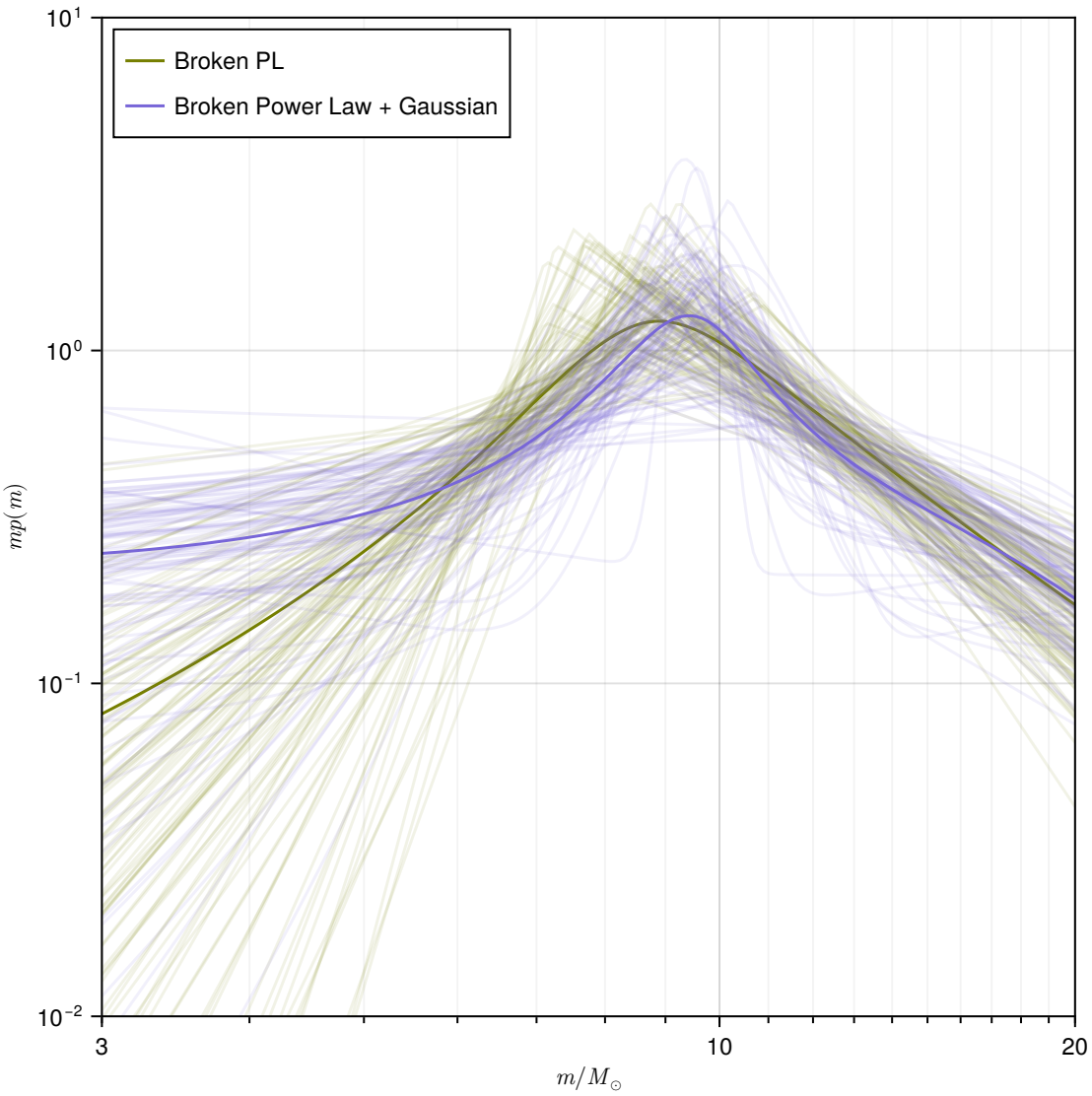

Figure 3. Inferred common mass distribution, $p(m)$, (see Eq. (9)) for both models considered in this analysis. Dark lines show the posterior mean mass distribution; light lines are individual draws from the posterior over mass distributions. At high masses, $m \gg \mu, m_b$, the mass function falls steeply in both models; the broken power law plus Gaussian slope $\alpha_2 = -2.5^{+1.4}_{-3.4}$. Toward lower masses from the peak, both power law models initially decline significantly, though the power law plus Gaussian model may rise again as $m \to 3\,M_\odot$.

BPL model which tries to fit the peak as well as the fall-offs using just two powerlaws. We however find consistency within measurement uncertainties between the BPL and BPLG models.

In Fig. 4, we show our posterior distribution for the first percentile of BH masses which are found to peak near and have significant support at $m = m_{\rm low}$, and in table 1 the corresponding 90% highest posterior density credible intervals. The BPLG model yields a much tighter constraint on $m_{1\%}$ and has no posterior support for the minimum

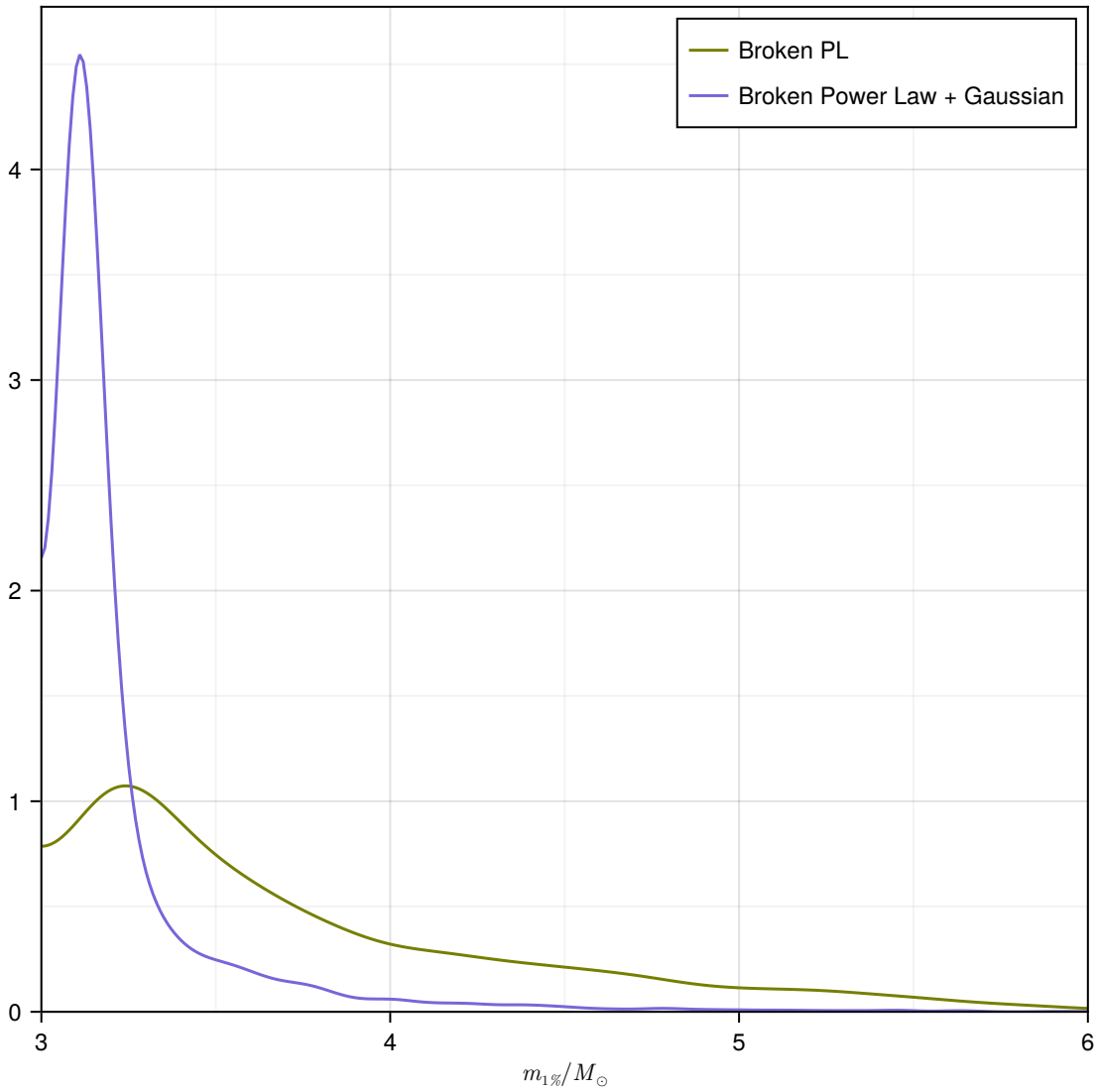

Figure 4. The posterior distribution for $m_{1\%}$, the first percentile of the "common" mass function for our three models. The broken power law plus Gaussian model with 50% selection cut has $m_{1\%} = 3.13^{+0.23}_{-0.05}\,M_\odot$ at 1σ (68%) credibility. The solid lines are the result for the 50% selection cut, dashed for the 90% selection cut.

BH mass to be above $3.6M_\odot$. In other words, BPLG model rules out the existence of a lower mass gap in our sample of low mass BHs with 90% posterior probability while the BPL model does not necessitate a gap but may permit one.

To explore the existence of any systematic biases arising from an arbitrarily chosen $m_{\rm low}$, which describes the boundary between the neutron star and black hole mass functions in our models, we look at variations in the measured $m_{1\%}$ values when the fixed $m_{\rm low}$ value is taken to be something in the range $(2.5M_\odot, 3.5M_\odot)$, which is shown in Fig. 5. We find that the peak of the posterior closely follows the location of $m_{\rm low}$, which indicates the absence of a lower mass-gap for all $m_{\rm low}$ values chosen. Both

Table 1. $m_{1\%}$ for our various models and using different selection functions.

Mass Function Model	$m_{1\%}/M_\odot$ (90%)	$m_{1\%}/M_\odot$ range (90%)
`Broken PL`	$3.24^{+1.52}_{-0.18}$	$[3.1, 4.8]$
`Broken Power Law + Gaussian`	$3.10^{+0.39}_{-0.08}$	$[3.0, 3.5]$

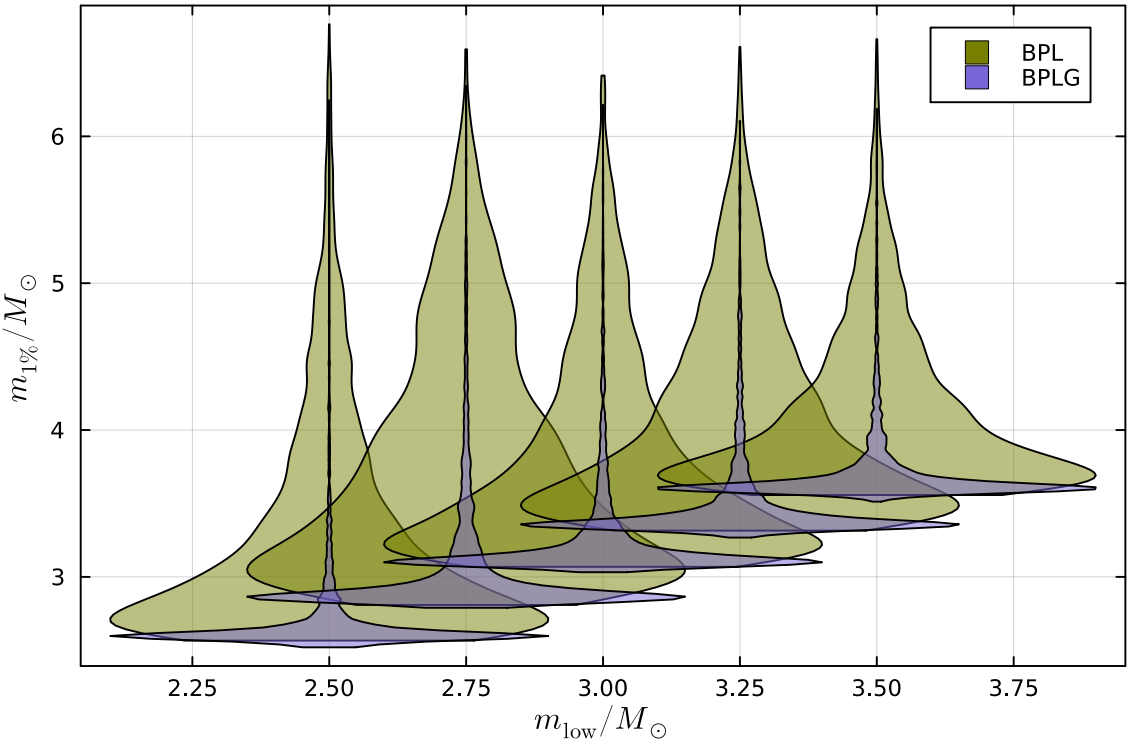

Figure 5. The posterior for $m_{1\%}$, corresponding to different values of $m_{\rm low}$ for the BPLG model in the form of violin plots.

models yield more constrained and peaked posteriors for smaller values of $m_{\rm low}$. We see the posteriors start to grow broader with increasing $m_{\rm low}$. The broadening of the posterior for $m_{\rm low} < 3M_\odot$ as well as the location of its peak is expected since in that range the secondary component of GW190814 (Abbott et al. 2020) stops contributing to the BH mass function for $m_{\rm low} > 2.7M_\odot$, at which point the $m_{1\%}$ inference is driven by the primary component of GW230529_181500. For $m_{\rm low} > 3.25M_\odot$, posterior samples of GW230529_181500 start getting excluded leading to weaker inference of the mass distribution in the lower end since that is the only event that contributes dominantly to the inference.

4. DISCUSSION

We have constrained the minimum BH mass using GW observations of CBC systems at least one of whose components is a BH. Using flexibly parametrized population

models and a mass cut to filter out BNS and high mass BBH events, we find the posterior distribution of the first percentile of the BH mass function to be 90% within $3.13^{+0.23}_{-0.05}\,M_\odot$for our most flexible model (broken power-law with a Gaussian peak). Our methodology justifies a direct comparison with LMXB-based probes of the lower mass gap modulo their treatment of selection effects. We find that for our most flexible population model, the existing sample of GW detections does not exhibit a lower mass gap in contrast to LMXB-based measurements, which can indicate the latter to be Malmquist biased (Siegel et al. 2023). For our less flexible model, however, we find that the current sample of GW detections does not require a gap but may permit one, with the $m_{1\%}$ posterior having small yet non-vanishing support near $5M_\odot$.

In addition to transient LMXB selection effects, an alternative explanation for this discrepancy is plausible. Merging BBH and NSBH systems with BHs in the lower mass gap can form through several scenarios such as hierarchical mergers in multiple systems (Lu et al. 2020; Liu & Lai 2021), dynamical encounters in young metal-rich stellar clusters (Arca Sedda 2021), non-segregated clusters (Clausen et al. 2014; Fragione & Banerjee 2020; Rastello et al. 2020), and near active galactic nuclei (McKernan et al. 2020; Yang et al. 2020), and massive stellar binaries (Antoniadis et al. 2022), that are not expected to yield LMXB systems. Identifying the contributions of these specific evolutionary pathways to low mass NSBH and BBH formation might necessitate the inference of higher dimensional population distributions that model not only the mass spectrum but also its correlations with other CBC parameters such as component spin magnitudes and orientations. However, given the small number of events in the lower gap, such an inference is likely to be uninformative given current datasets and is hence left as a future exploration.

In accordance to existing studies (e.g., Abbott et al. 2023a; Abac et al. 2024; Tiwari 2022; Farah et al. 2023; Ray et al. 2023; Sadiq et al. 2024; Edelman et al. 2023; Callister & Farr 2024; Ray et al. 2023, 2024; Heinzel et al. 2025), we also recover an excess of BHs near $m = 9.31^{+0.73}_{-0.93}\,M_\odot$, with the merger rate density at the location of the being $96^{+119}_{-52}\,\mathrm{Gpc}^{-3}\,\mathrm{yr}^{-1}$per log mass squared. We further characterize the fall-off in the merger rate density on either side of the peak. In particular, we find that in the low-mass end, the maximum fall-off compared to the peak is less than an order of magnitude, with the rate density at $3M_\odot$ being $18^{+28}_{-12}\,\mathrm{Gpc}^{-3}\,\mathrm{yr}^{-1}$per log mass squared. We note that while various population models used in previous analyses have identified these features individually, we are able to reconstruct both simultaneously using a single mass model, thereby showing that the data is consistent with a mass function that has a relatively strong peak near $10M_\odot$ and a very shallow fall-off in merger rate density towards the lower end of said peak, right up to the NS region of the parameter space.

The presence of both a strong peak and a shallow drop in merger rate density towards the lower end of the BH mass spectrum has interesting astrophysical implications. Several models of compact binary formation, such as isolated stellar binaries

undergoing stable mass transfer without a common envelope phase (van Son et al. 2022), can explain this abundance of $8-10M_\odot$ BBHs or the shallow gap between NSs and BHs individually. For this particular formation channel, van Son et al. (2022) demonstrate that the astrophysical prescriptions that give rise to a strong peak near $10M_\odot$ also predict a very sharp fall of in merger rate density, which can drop by several orders of magnitude even above $4M_\odot$. On the other hand, the physical assumptions that are consistent with a very shallow drop in merger rate density predict no significant over-abundance of BBHs in the $8-10M_\odot$ range. In other words, any single channel modeled by van Son et al. (2022) to explore the stable mass-transfer-only formation scenario cannot fully explain the shape of the BH mass function that we find in the lower end. If one were to assume that van Son et al. (2022) have exhaustively and accurately explored the stable-mass-transfer scenario, then our results could indicate substantial contributions from other formation channels, such as common-envelope evolution followed by stable mass transfer or dynamical encounters, to the observed population of low mass BHs.

5. ACKNOWLEDGEMENTS

We thank Jeff Andrews for comments on an early version of this work. This work was initiated at the Aspen Center for Physics, which is supported by National Science Foundation grant PHY-2210452. This research was also supported in part through the computational resources and staff contributions provided for the Quest high-performance computing facility at Northwestern University, which is jointly supported by the Office of the Provost, the Office for Research, and Northwestern University Information Technology. Some computations in this work were, in part, run at facilities supported by the Scientific Computing Core at the Flatiron Institute, a division of the Simons Foundation. A.R. was supported by the National Science Foundation (NSF) award PHY-2207945. V.K. was supported by the Gordon and Betty Moore Foundation (grant awards GBMF8477 and GBMF12341), through a Guggenheim Fellowship, and the D.I. Linzer Distinguished University Professorship fund. W.F. is partially supported by the Center for Computational Astrophysics, part of the Flatiron Institute, a division of the Simons Foundation. The authors are grateful for computational resources provided by the LIGO Laboratory and supported by NSF Grants No. PHY-0757058 and No. PHY0823459. V.K. and A.R. gratefully acknowledge the support of the NSF-Simons AI-Institute for the Sky (SkAI) via grants NSF AST-2421845 and Simons Foundation MPS-AI-00010513. This material is based upon work supported by NSF's LIGO Laboratory which is a major facility fully funded by the National Science Foundation. This research has made use of data obtained from the Gravitational Wave Open Science Center (gwosc.org), a service of LIGO Laboratory, the LIGO Scientific Collaboration, the Virgo Collaboration, and KAGRA.

Software: `Makie.jl` (Danisch & Krumbiegel 2021); `Turing.jl` (Ge et al. 2018); `zenodo-get` (Völgyes 2020)

REFERENCES

Aasi, J., et al. 2015, Class. Quant. Grav., 32, 074001, doi: 10.1088/0264-9381/32/7/074001

Abac, A. G., et al. 2024, Astrophys. J. Lett., 970, L34, doi: 10.3847/2041-8213/ad5beb

Abbott, R., et al. 2020, Astrophys. J. Lett., 896, L44, doi: 10.3847/2041-8213/ab960f

—. 2021, Phys. Rev. X, 11, 021053, doi: 10.1103/PhysRevX.11.021053

—. 2023a, Phys. Rev. X, 13, 011048, doi: 10.1103/PhysRevX.13.011048

—. 2023b, Phys. Rev. X, 13, 041039, doi: 10.1103/PhysRevX.13.041039

—. 2023c, Open data from the third observing run of LIGO, Virgo, KAGRA and GEO. https://arxiv.org/abs/2302.03676

Acernese, F., et al. 2015, Class. Quant. Grav., 32, 024001, doi: 10.1088/0264-9381/32/2/024001

Ai, S., Gao, H., & Zhang, B. 2019, doi: 10.3847/1538-4357/ab80bd

Akutsu, T., et al. 2021, PTEP, 2021, 05A102, doi: 10.1093/ptep/ptab018

Alsing, J., Silva, H. O., & Berti, E. 2018, MNRAS, 478, 1377, doi: 10.1093/mnras/sty1065

Antoniadis, J., Aguilera-Dena, D. R., Vigna-Gómez, A., et al. 2022, Astron. Astrophys., 657, L6, doi: 10.1051/0004-6361/202142322

Arca Sedda, M. 2021, Astrophys. J. Lett., 908, L38, doi: 10.3847/2041-8213/abdfcd

Bailyn, C. D., Jain, R. K., Coppi, P., & Orosz, J. A. 1998, Astrophys. J., 499, 367, doi: 10.1086/305614

Belczynski, K., Wiktorowicz, G., Fryer, C., Holz, D., & Kalogera, V. 2012, Astrophys. J., 757, 91, doi: 10.1088/0004-637X/757/1/91

Callister, T. A., & Farr, W. M. 2024, Phys. Rev. X, 14, 021005, doi: 10.1103/PhysRevX.14.021005

Clausen, D., Sigurdsson, S., & Chernoff, D. F. 2014, Mon. Not. Roy. Astron. Soc., 442, 207, doi: 10.1093/mnras/stu871

Danisch, S., & Krumbiegel, J. 2021, Journal of Open Source Software, 6, 3349, doi: 10.21105/joss.03349

Edelman, B., Farr, B., & Doctor, Z. 2023, Astrophys. J., 946, 16, doi: 10.3847/1538-4357/acb5ed

Essick, R., & Farr, W. 2022, Precision Requirements for Monte Carlo Sums within Hierarchical Bayesian Inference. https://arxiv.org/abs/2204.00461

Ezquiaga, J. M., & Holz, D. E. 2022, Phys. Rev. Lett., 129, 061102, doi: 10.1103/PhysRevLett.129.061102

Farah, A. M., Edelman, B., Zevin, M., et al. 2023, Astrophys. J., 955, 107, doi: 10.3847/1538-4357/aced02

Farah, A. M., Fishbach, M., Essick, R., Holz, D. E., & Galaudage, S. 2022, Astrophys. J., 931, 108, doi: 10.3847/1538-4357/ac5f03

Farr, W. M. 2019, Research Notes of the AAS, 3, 66, doi: 10.3847/2515-5172/ab1d5f

Farr, W. M., & Chatziioannou, K. 2020, Research Notes of the American Astronomical Society, 4, 65, doi: 10.3847/2515-5172/ab9088

Farr, W. M., Sravan, N., Cantrell, A., et al. 2011, Astrophys. J., 741, 103, doi: 10.1088/0004-637X/741/2/103

Fishbach, M., & Holz, D. E. 2020, ApJL, 891, L27, doi: 10.3847/2041-8213/ab7247

Fragione, G., & Banerjee, S. 2020, Astrophys. J. Lett., 901, L16, doi: 10.3847/2041-8213/abb671

Fryer, C. L., Belczynski, K., Wiktorowicz, G., et al. 2012, Astrophys. J., 749, 91, doi: 10.1088/0004-637X/749/1/91

Fryer, C. L., & Kalogera, V. 2001, Astrophys. J., 554, 548, doi: 10.1086/321359

Fryer, C. L., Olejak, A., & Belczynski, K. 2022, Astrophys. J., 931, 94, doi: 10.3847/1538-4357/ac6ac9

Ge, H., Xu, K., & Ghahramani, Z. 2018, in International Conference on Artificial Intelligence and Statistics, AISTATS 2018, 9-11 April 2018, Playa Blanca, Lanzarote, Canary Islands, Spain, 1682–1690. http://proceedings.mlr.press/v84/ge18b.html

Heinzel, J., Mould, M., & Vitale, S. 2025, Phys. Rev. D, 111, L061305, doi: 10.1103/PhysRevD.111.L061305

Homan, M. D., & Gelman, A. 2014, J. Mach. Learn. Res., 15, 1593–1623

Kabán, A. 2012, Stat. Comput., 22, 375

Kalogera, V., & Baym, G. 1996, Astrophys. J. Lett., 470, L61, doi: 10.1086/310296

Kreidberg, L., Bailyn, C. D., Farr, W. M., & Kalogera, V. 2012, Astrophys. J., 757, 36, doi: 10.1088/0004-637X/757/1/36

LIGO Scientific Collaboration, KAGRA Collaboration, & Virgo Collaboration. 2024, LVK data release for GW230529_181500 event, Gravitational Wave Open Science Center, doi: 10.7935/6K89-7Q62

Liotine, C., Zevin, M., Berry, C. P. L., Doctor, Z., & Kalogera, V. 2023, The Astrophysical Journal, 946, 4, doi: 10.3847/1538-4357/acb8b2

Liu, B., & Lai, D. 2021, Mon. Not. Roy. Astron. Soc., 502, 2049, doi: 10.1093/mnras/stab178

Liu, T., Wei, Y.-F., Xue, L., & Sun, M.-Y. 2021, Astrophys. J., 908, 106, doi: 10.3847/1538-4357/abd24e

Loredo, T. J. 2004, in AIP Conference Proceedings (AIP), doi: 10.1063/1.1835214

Lu, W., Beniamini, P., & Bonnerot, C. 2020, Mon. Not. Roy. Astron. Soc., 500, 1817, doi: 10.1093/mnras/staa3372

Madau, P., & Dickinson, M. 2014, ARA&A, 52, 415, doi: 10.1146/annurev-astro-081811-125615

Mandel, I., Farr, W. M., & Gair, J. R. 2019, Mon. Not. Roy. Astron. Soc., 486, 1086, doi: 10.1093/mnras/stz896

Mandel, I., & Müller, B. 2020, Mon. Not. Roy. Astron. Soc., 499, 3214, doi: 10.1093/mnras/staa3043

Margalit, B., & Metzger, B. D. 2017, The Astrophysical Journal Letters, 850, L19, doi: 10.3847/2041-8213/aa991c

McKernan, B., Ford, K. E. S., & O'Shaughnessy, R. 2020, Mon. Not. Roy. Astron. Soc., 498, 4088, doi: 10.1093/mnras/staa2681

Mueller, H., & Serot, B. D. 1996, Nucl. Phys. A, 606, 508, doi: 10.1016/0375-9474(96)00187-X

Neal, R. M. 2011, in Handbook of Markov Chain Monte Carlo, ed. S. Brooks, A. Gelman, G. Jones, & X.-L. Meng (Chapman and Hall/CRC), doi: 10.1201/b10905

Özel, F., & Freire, P. 2016, Ann. Rev. Astron. Astrophys., 54, 401, doi: 10.1146/annurev-astro-081915-023322

Ozel, F., Psaltis, D., Narayan, R., & McClintock, J. E. 2010, Astrophys. J., 725, 1918, doi: 10.1088/0004-637X/725/2/1918

Patton, R. A., Sukhbold, T., & Eldridge, J. J. 2022, Mon. Not. Roy. Astron. Soc., 511, 903, doi: 10.1093/mnras/stab3797

Raaijmakers, G., Greif, S. K., Hebeler, K., et al. 2021, Astrophys. J. Lett., 918, L29, doi: 10.3847/2041-8213/ac089a

Rastello, S., Mapelli, M., Di Carlo, U. N., et al. 2020, Mon. Not. Roy. Astron. Soc., 497, 1563, doi: 10.1093/mnras/staa2018

Ray, A., Magaña Hernandez, I., Breivik, K., & Creighton, J. 2024. https://arxiv.org/abs/2404.03166

Ray, A., Magaña Hernandez, I., Mohite, S., Creighton, J., & Kapadia, S. 2023, Astrophys. J., 957, 37, doi: 10.3847/1538-4357/acf452

Rhoades, C. E., & Ruffini, R. 1974, Phys. Rev. Lett., 32, 324, doi: 10.1103/PhysRevLett.32.324

Roy, S. K., van Son, L. A. C., & Farr, W. M. 2025. https://arxiv.org/abs/2507.01086
Sadiq, J., Dent, T., & Gieles, M. 2024, Astrophys. J., 960, 65, doi: 10.3847/1538-4357/ad0ce6
Saw, J. G., Yang, M. C., & Mo, T. C. 1984, The American Statistician, 38, 130, doi: 10.1080/00031305.1984.10483182
Shao, D.-S., Tang, S.-P., Jiang, J.-L., & Fan, Y.-Z. 2020, Phys. Rev. D, 102, 063006, doi: 10.1103/PhysRevD.102.063006
Siegel, J. C., et al. 2023, Astrophys. J., 954, 212, doi: 10.3847/1538-4357/ace9d9
Talbot, C., & Golomb, J. 2023, MNRAS, 526, 3495, doi: 10.1093/mnras/stad2968
Thrane, E., & Talbot, C. 2019, Publ. Astron. Soc. Austral., 36, e010, doi: 10.1017/pasa.2019.2
Tiwari, V. 2022, Astrophys. J., 928, 155, doi: 10.3847/1538-4357/ac589a
van Son, L. A. C., de Mink, S. E., Renzo, M., et al. 2022, Astrophys. J., 940, 184, doi: 10.3847/1538-4357/ac9b0a
Vitale, S., Gerosa, D., Farr, W. M., & Taylor, S. R. 2020, doi: 10.1007/978-981-15-4702-7_45-1
Völgyes, D. 2020, Zenodo_get: a downloader for Zenodo records., doi: 10.5281/zenodo.1261812
Wysocki, D., Lange, J., & O'Shaughnessy, R. 2019, Phys. Rev. D, 100, 043012, doi: 10.1103/PhysRevD.100.043012
Yang, Y., Gayathri, V., Bartos, I., et al. 2020, Astrophys. J. Lett., 901, L34, doi: 10.3847/2041-8213/abb940
Zevin, M., Spera, M., Berry, C. P. L., & Kalogera, V. 2020, Astrophys. J. Lett., 899, L1, doi: 10.3847/2041-8213/aba74e